We are IntechOpen, the world's leading publisher of Open Access books Built by scientists, for scientists

6,900
Open access books available

186,000
International authors and editors

200M
Downloads

Our authors are among the

154
Countries delivered to

TOP 1%
most cited scientists

12.2%
Contributors from top 500 universities

WEB OF SCIENCE™

Selection of our books indexed in the Book Citation Index in Web of Science™ Core Collection (BKCI)

Interested in publishing with us?
Contact book.department@intechopen.com

Numbers displayed above are based on latest data collected.
For more information visit www.intechopen.com

Chapter

Ultrasonic Processing of Si and SiGe for Photovoltaic Applications

Andriy Nadtochiy, Artem Podolian, Oleg Korotchenkov and Viktor Schlosser

IntechOpen

Abstract

The usage of power ultrasound for sonochemical processing of Si wafers and thin layers of amorphous Si and SiGe alloys is described. Over the last decade different industries have become increasingly drawn to sonochemistry because it provides a green and clean alternative to conventional technologies, particular in the areas of processing of silicon-based materials for photovoltaic applications. Two techniques related to ultrasonic cleaning of Si wafers and sonochemical modification of Si, SiGe and a-Si/SiGe surfaces in hydrocarbon solutions of chloroform ($CHCl_3$) and dichloromethane (CH_2Cl_2) are discussed. The occurrence of cavitation and bubble implosion is an indispensable prerequisite for ultrasonic cleaning and surface processing as it is known today. The use of higher ultrasonic frequencies to expand the range of ultrasonic cleaning and processing capabilities is emphasized. Although exact mechanisms of an improved photoelectric behavior of Si-based structures subjected to power ultrasound are not yet clarified in many cases, the likely scenarios behind the observed photovoltaic performances of Si, SiGe and a-Si/SiGe surfaces are proposed to involve the surface chemistry of oxygen and hydrogen molecules as well hydrocarbon chains.

Keywords: silicon, germanium, surface passivation, dichloromethane, sonochemical, surface photovoltage, free carrier lifetimes

IntechOpen

1. Introduction

The chemical effect of ultrasonic waves derives primarily from hot spots formed during acoustic cavitation in a chemical mixture. Due to locally achieved extreme conditions, an unusual chemical environment is attained in such experiments [1]. It is therefore not surprising that a growing interest in simple and cheap sonochemical syntheses of materials is observed, particularly in nanophases [2–4]. Given the fact that ultrasonic irradiation, or sonication, of reaction mixtures is easily controllable, sonochemical fabrication of high-quality materials becomes a particularly interesting subject. One of the goals of this article is to discuss the recent excitement about sonochemically modified semiconductor materials.

Quite recently, sonochemical techniques have been used in processing of semiconductor surfaces [5–14]. In this method, the main phenomenon is the acoustic cavitation, which enhances chemical reactions in a solution. The growth of cavitation bubbles occurs due to the diffusion of solute vapor in the volume of the bubbles. After the growth process, the bubbles collapse, breaking the chemical bonds on the material surface.

Over the last years different industries have therefore become increasingly drawn to sonochemistry because it provides a green and clean alternative to conventional technologies, particular in the areas of processing of silicon-based materials. The aim of this work is to provide a cohesive presentation of the related efforts. Two techniques related to ultrasonic cleaning of Si wafers and sonochemical modification of Si and SiGe surfaces in hydrocarbon solutions will be discussed. In both cases, the occurrence of cavitation and bubble implosion is necessary for ultrasonic cleaning and surface processing as it is known today. The use of higher ultrasonic frequencies to expand the range of ultrasonic cleaning and processing capabilities will be emphasized. Although exact mechanisms of an improved photoelectric behavior of Si-based micro- and nanostructures subjected to power ultrasound are not yet clarified in many cases, the likely scenarios behind the observed photovoltaic performances will be proposed to involve the surface chemistry of oxygen and hydrogen molecules as well hydrocarbon chains.

2. Processing and passivation of Si wafers used for solar cells

It is known that crystalline silicon (c-Si) based solar cells dominate the solar energy industry. The modern silicon wafer production technology and processing sequence is the most mature and including hundreds of flawless process steps [15]. With increasing the electronic quality of c-Si, the efficiency of c-Si solar cells improved considerably [16]. Most generally, free carriers generated by the incident sunlight would be efficiently collected far away from the fast recombination centers while they move towards the device terminals. In particular, carrier recombination at the cell surfaces should be avoided, especially in thin wafers.

It is convenient to define an effective surface recombination velocity (S_{eff}), which for a symmetrically passivated sample at a low injection level takes the form [17]:

$$S_{eff} = \sqrt{D\left(\frac{1}{\tau_{eff}} - \frac{1}{\tau_b}\right)} \tan\left(\frac{w}{2}\sqrt{\frac{1}{D}\left(\frac{1}{\tau_{eff}} - \frac{1}{\tau_b}\right)}\right), \tag{1}$$

where D is the minority carrier diffusivity, τ_{eff} is the effective lifetime, τ_b is the bulk lifetime of the wafer and w is the wafer thickness. If S_{eff} is rather large, one equates [17]:

$$\frac{1}{\tau_{eff}} = \frac{1}{\tau_b} + D\left(\frac{\pi}{w}\right)^2. \tag{2}$$

If the surface passivation is good and hence the surface recombination velocity is sufficiently small, the tangent term in Eq. (1) becomes linear and [17]:

$$\frac{1}{\tau_{eff}} = \frac{1}{\tau_b} + \frac{2S_{eff}}{w}. \tag{3}$$

Therefore, carrier recombination at the wafer surfaces restricts its effective lifetime thus posing inherent limitation of using c-Si in solar cells.

The surface itself terminates an atomic order in c-Si such that Si atoms that reside on the surface are not fully bonded to four Si neighbors. This yields dangling bonds, which form surface defects and thus reduce the efficiency of solar cells. Therefore, reducing the number of these defects is clearly a necessary prerequisite for manufacturing higher efficiency silicon solar cells.

In this respect, various surface-passivation layers have been employed. In particular, SiO_2 surface passivation coating layer has been proven to offer outstanding passivation [18–20]. In general, two oxide growth methods are employed termed as the dry and wet oxidation. Dry oxygen and water vapor are used in the former and latter cases, respectively. Dry oxidation typically forms thin oxide layers in practical structures due to perfect Si–SiO_2 interface developed in this case. In turn, wet oxidation yields greater growth rates, which is necessary for depositing thicker SiO_2 layers.

Furthermore, a hydrogenated amorphous silicon a-Si:H layer can saturate the dangling bonds by hydrogen termination [21–23]. The atomic hydrogen is also able to effectively passivate dangling bonds at the c-Si/SiO_2 interface thus drastically suppressing the interface state density and surface recombination velocities [24]. An important aspect is that the treatment in HF can produce an inversion layer on p-type Si surfaces while an accumulation of majority carriers is observed on n-type Si after treatment in either NH_4F or HF [25]. These both are due to positive charges induced by electronegative surface groups such as –H, –O–H and –F bonded to the Si surface atoms $\equiv Si_s-$ [26].

Most of the oxidizing solutions, e.g. H_2SO_4/H_2O_2, HCl, HNO_3, RCA-2 (the mixture of HCl, H_2O_2 and H_2O), lead to surface depletion of holes in p-Si and a weakly depleted majority carriers in n-Si that appear due to the positive fixed oxide charge. Surface processing in the RCA-1 solution, which contains the mixture of NH_4OH, H_2O_2 and H_2O, can be considered, in turn, noting a strong depletion in n-Si and a weak one on p-type Si surface thus implying the negative surface charge arisen from the dissociation of ≡Si–OH groups in the SiO_2 film during the oxidation in the solution ($\equiv Si–OH \leftrightarrows \equiv Si–O^- + H^+$) [25, 26].

Using an amorphous silicon layer should also prove useful in Ge_xSi_{1-x}/Si structures [27]. It is seen in **Figure 1** that the surface photovoltage (SPV) is enhanced as the structure is covered with a-Si (curves 3 and 4 compared with curves 1 and 2 at time $t = 0$). Roughly a 10 times larger value of the SPV magnitude is observed in the

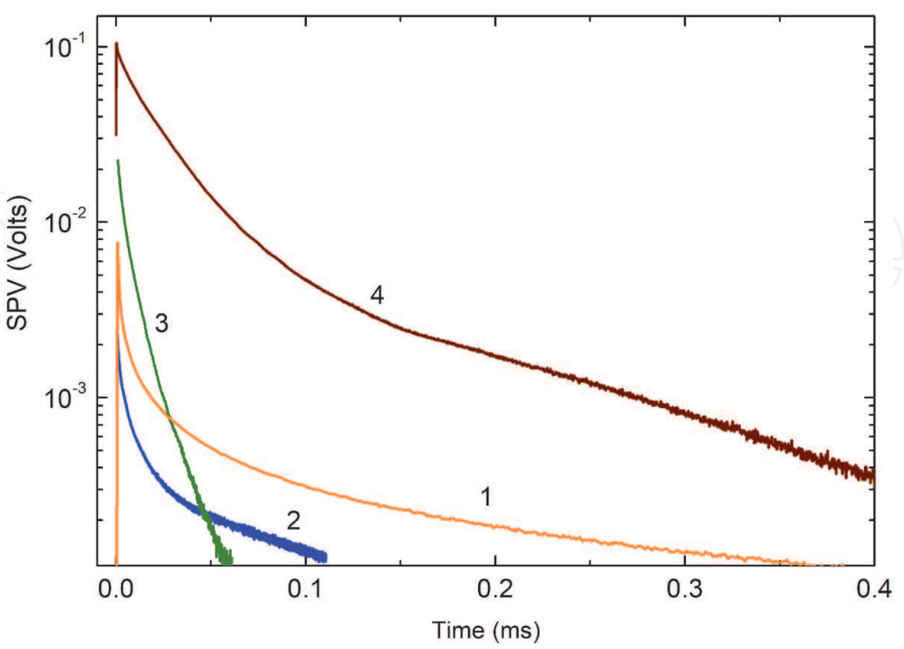

Figure 1.
Time-dependent SPV of Si wafer (1), structures of Ge_xSi_{1-x} islands on Si (2), 10 nm a-Si/Ge_xSi_{1-x}/Si (3), and 10 nm a-Si/Ge_xSi_{1-x}/Si annealed for 5 minutes at 400 °C in an O_2 ambient atmosphere (4). The concentration of Ge atoms in the islands is about 80%. Reprinted with permission from Podolian A, Nadtochiy A, Korotchenkov O, Romanyuk B, Melnik V, Popov V. Journal of Applied Physics. 2018;124:095703. Copyright 2018, AIP publishing.

capped Ge_xSi_{1-x}/Si structure (curve 3 at time $t = 0$) compared to that of bare Ge_xSi_{1-x}-on-Si islands (curve 2). This enlargement is even 5 to 10 times greater after subsequent sample annealing in O_2 (curve 4 at time $t = 0$).

Presuming the use of effective hydrogenation, a-Si:H/c-Si heterojunction solar cells (HET) represent one of the most promising solar cell structures that enable high efficiencies due to high open-circuit values coming from the excellent passivation properties of a-Si:H combined with the beneficial effect of the *a*-Si:H/c-Si heterojunction on the built-in voltage and reduced charge carrier loss at the interface [28]. HET cells also have reduced costs compared with systems installed today based on conventional silicon technologies.

Moreover, in contrast to dielectric passivation materials such as SiO_2 and amorphous Si nitride (a-SiN_x:H) [29], a-Si:H is simultaneously suitable for good passivation and electrical conduction. However, the surface passivation quality worsens both at low and high processing temperatures because of the porous medium grown in the amorphous silicon phase at excess amounts of hydrogen [30] and growing crystalline Si film instead of forming a-Si:H [31, 32], respectively. As a consequence, discrepancy exists in the literature as to the passivation ability of a-Si:H [33–37].

3. Sonochemistry: basic principles

The use of ultrasound for accelerating chemical reactions in liquid–solid heterogeneous systems is very attractive since ultrasound is capable of increasing the reactivity by more than a factor of 10^5 due to the fact that the reagent particles clash at such a high speed that they melt at the point of collision and generate microscopic flames in cold liquids [1, 38]. In ultrasonically irradiated slurries, turbulent flow and shock waves are produced by acoustic cavitation [39] resulting in many tiny gas bubbles. The bubbles expand and contract in accordance with the pressure oscillations of the ultrasonic wave. When the bubble radius is of a certain size and the acoustic amplitude is above a given threshold value, the bubbles collapse violently and the temperature inside a bubble increases dramatically due to the quasiadiabatic compression [40]. At the final stage of the collapse, the vapor, which often is water vapor, dissociates inside the collapsing bubble due to the high bubble temperature. This generates H and OH radicals as well as other kinds of oxidants, which are assumed to produce a variety of chemical reactions [3, 41–45]. The reactions involve the formation of primary radicals from the ultrasound-initiated dissociation of water within a collapsing cavity as

$$H_2O))) \rightarrow H + OH, \tag{4}$$

where the brackets stand for the sonolysis of water. The intermediate hydroxyl and hydrogen radicals can form H_2O_2 and O_2 products.

In aqueous media, these reactions occur in different regions surrounding the collapsed bubble. One of these regions is e.g. the interfacial liquid region between the cavitation bubbles and the bulk solution. The temperature in this region is lower than the one in the interior of the bubbles. The reaction is therefore a liquid phase reaction but the temperature is believed to be high enough to rupture chemical bonds. Apart from these oxidants, considerable concentrations of local hydroxyl radical have been reported [43, 46]. Another reactant region is the bulk solution. Here, the reaction between reactant molecules and OH or H takes place at ambient temperatures.

Since a quantitative analysis of the chemistry involved into the sonochemical reactions is yet difficult to perform [47], it is not certain whether or not the chemical effects indeed originate from acoustic cavitation. The implosive collapse of

bubbles during cavitation produces local transient temperatures of about 5000 K and pressures of about 500 atm, with heating and cooling rates exceeding 10^{10} K/s [1, 38]. These conditions create high-velocity collisions between suspended particles and the estimated speed of colliding particles approaches almost the speed of sound in the liquid. Interestingly, sonochemical reactions in cavitational fields occur more slowly at elevated than at lower temperatures. Even so it is surprising, this counterintuitive property makes sense, because at higher temperatures more solvents vaporize into the bubble and, hence, cushion the collapse.

In cold liquids, ultrasound is able to drive reactions that normally occur only under extreme conditions. Examples [45] include intercalation, activation of liquid–solid reactions, and the synthesis of amorphous and nanophase materials. The sonochemical syntheses of nanophase metals, alloys, metal carbides, supported heterogeneous catalysts, and nano-colloids derives from the sonochemical decomposition of volatile organo-metallic precursors during cavitation, which produces clusters of a few nm in diameter.

Various types of sonochemical cells using ultrasound baths and ultrasound horn systems have been reported [48–50]. Most frequently, an ultrasonic transducer and the ultrasound horn are placed directly in the solution. One example is shown in **Figure 2**. An oscillating rf voltage from an oscillator (1 in **Figure 2**) with the amplitude of U_0 is amplified by an amplifier (2) and applied to a Langevin transducer, which consists of a piezoelectric transducer (3), back (4) and front (5) masses. The vibrating transducer is loaded to a glass flask (6) filled with a reactant solution (7) thus delivering an acoustic power at a resonance frequency of the transducer-solution system. The lowest-mode resonance frequency is defined by the solution thickness h such that $h = \lambda/2$ with λ the sound wavelength in the solution at the resonant frequency.

The samples can freely levitate near the pressure antinode zone at operating frequencies in the dozens kHz range. They tend to reside on the flask bottom when increasing the frequency up to several hundreds of kHz.

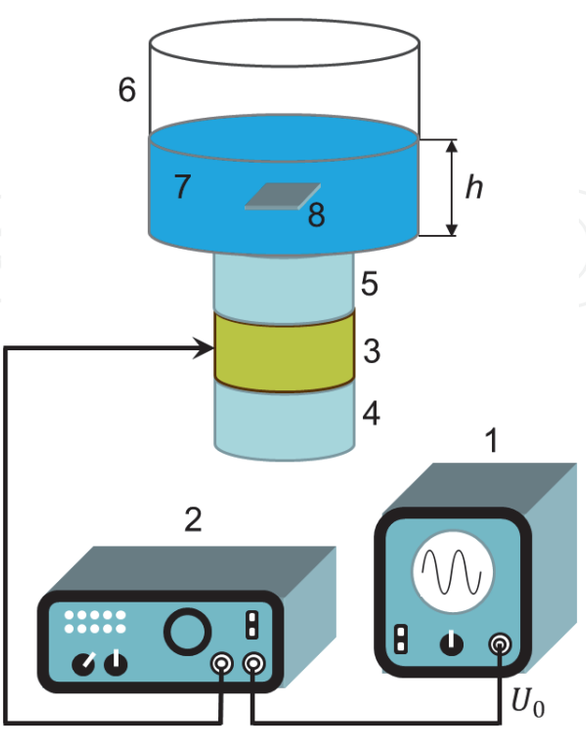

Figure 2.
Schematic of the sonochemical cell: 1 – Oscillator, 2 – Amplifier, 3 – Piezoelectric transducer, 4 – Back mass, 5 – Front mass, 6 – Boiling flask, 7 – Reactant solution, 8 – Sample.

4. Ultrasonic cleaning of Si wafers

Cleaning and conditioning of silicon wafer surfaces and Si/SiO_2 interfaces for the manufacturing of photovoltaic and microelectronic devices are in increasing demand with improved performance, reliability of these devices, scaling down to below 10 nm, incorporating extended metallization layers, employing epitaxial layers of compound SiGe and III-V semiconductors [51]. Clean wafer surfaces are crucial in high efficiency solar cell as well as in Ultra-Large Scale Integration (ULSI) fabrication processes, fin-shaped field effect transistors (FinFET), 3D NAND-stacked memory devices etc.

Deposition of monolayers and self-assembly of nanoparticles in multilevel structures requires the wafer surface to be completely free of any particulate contamination down to a nanometer scale. Moreover, installing a 1 MWp solar module generator implies that more than $2 \cdot 10^5$ Si wafers must be processed.

Furthermore, metallic contaminants on Si wafers cause substantial increase in leakage current in silicon p-n junctions and decrease the oxide breakdown voltage thus deteriorating the minority carrier lifetime [52, 53]. In particular, Cu and Al contaminants worsen the gate oxide integrity [54, 55]. To achieve ultraclean substrate surfaces with high reproducibility, it is also important to note that not only removal of contaminants is effective in improving the cell performance, but also prevention of their redeposition on the wafer surface. In this respect, dilute HF can be effectively used. However, some Cu and Al residues can be found on the wafer surface due to its hydrophobic nature [56].

The contamination of wafer surfaces by particle contaminants is one of the major problems in the industries. One way to increase the yield on fully processed silicon wafers is to use cleaning techniques specifically efficient to remove particle contaminants. Small particles are especially difficult to remove because they are strongly bounded to the substrate by electrostatic forces. It is therefore very important to find an effective way to remove particles from wafers without causing damage to the wafers.

A wide variety of cleaning methods are being used in wafer manufacturing such as brush or water-jet scrubbing of wafer surfaces employed prior to further immersion-type cleaning, scrubbing of rotating wafer surfaces between each processing step, adding cheating agents to the solution aiming to avoid metal adsorption onto Si wafers, cleaning in wet chemical baths, post treatment rinsing and many others [57]. They, however, are known to damage the wafer surface. Moreover, the chemical-type cleaning has inherent danger caused by residues from sulfuric acid, ammonium hydroxide, isopropyl alcohol and other chemical pollutants. For example, an immersion-type cleaning step widely used industrially utilizes RCA Standard Clean 1 (RCA-1) [58].

Wet-chemical processes are still the most widely used method for Si wafer cleaning in the semiconductor industry today [51]. The critical demands of surface purity raised by the International Technology Roadmap for Semiconductors (ITRS) [59] can generally be reduced by utilizing ultrasonic cleaning processes.

In the above context, a substrate independent cleaning process is highly desirable because, opposite to a chemical based cleaning process, it is equally well suited for different substrates and does not modify the surface through the etching, roughening, etc.

While keeping the compatibility with Si wafer standard processing steps, ultrasonic treatment of surfaces can be effective in passing several obstacles to achieving wafer cleaning mentioned above. Ultrasonic cleaning employs an ultrasonically activated liquid with a submerged wafer used to achieve or enhance the removal of surface contaminants [60]. Ultrasonic irradiation involves a variety of complex

mechanisms, including mechanical vibration and appropriate pressure gradients, microcavitation bubbles that oscillate and dance around due to Bjerknes force [39, 61], acoustic streaming flows, etc. One of the most important aspects of using acoustic streaming is the effect of the frequency on the boundary layer [62]. Its thickness decreases and the streaming velocity increases with increasing the sonication frequency. These both remarkably increase the drag force and hence the particle removal efficiency. It is demonstrated that the acoustic streaming induced removal of foreign contaminants with sizes in the dozen nm range is accomplished at frequencies greater than 1 MHz, i.e. in a high-frequency sonication region [63]. The removal of contaminants having sizes down to ≈100 nm is possible at frequencies smaller than 1 MHz [64].

It has furthermore been demonstrated that the caustic etching process can be ultrasonically enhanced producing finer, more homogeneous textured surfaces [65]. This technique inhibits the sunlight reflection from the Si surface thus enhancing the performance of solar cells.

To demonstrate the capabilities of high-power ultrasound in powerfully manipulating surface species, consider the data reported in **Figure 3**. Here, following the method of cleaning from laser-induced cavitation bubbles [66], the wafer surface is covered with a thin layer of grease. This yields the optical transmission spectra indicative of organic contaminants, which are marked by several peaks in spectra 2 of **Figure 3**, such as C–CH_3 at 2960 cm^{-1}, –CH_2– at 2920 cm^{-1}, –CH at 2890 cm^{-1} and C–H stretching vibrations [–CH_3 and –$(CH_2)_n$–] at 2850 cm^{-1} [67]. It is seen in spectra 3 that organic contaminants are effectively removed from the wafer surface upon its exposure to ultrasonic cavitation with the peak acoustic intensity of about

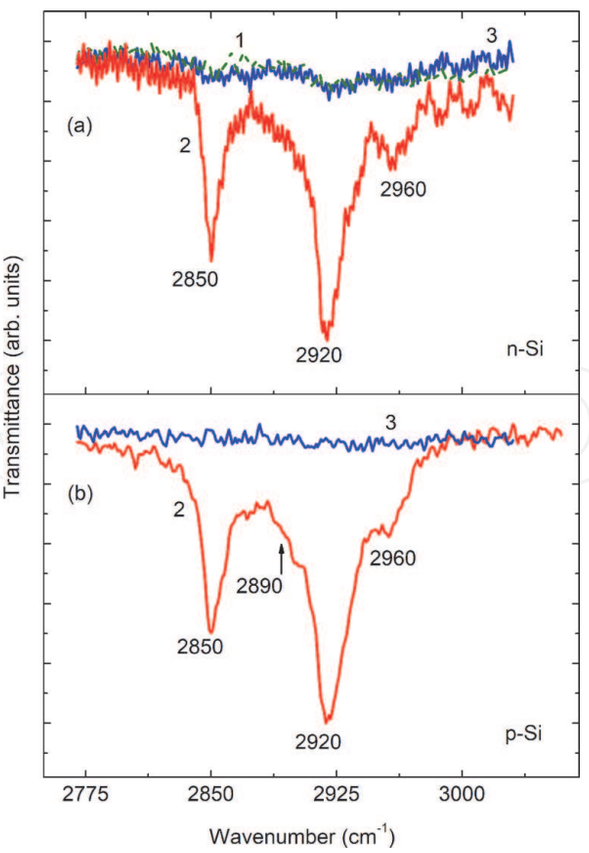

Figure 3.
FTIR spectra of n-Si (a) and p-Si (b) wafers, prior to surface greasing and applying the ultrasound (spectrum 1), covered with a thin layer of vaseline (2) and subsequently cleaned in an ultrasonic bath (3) during 15 min. Reprinted with permission from Podolian A, Nadtochiy A, Kuryliuk V, Korotchenkov O, Schmid J, Drapalik M, Schlosser V. Solar Energy Materials and Solar Cells. 2011;95:765–772. Copyright 2010, Elsevier.

400 W/cm^2 [68], so that the resulting absorption resembles the one taken before the wafer has been exposed to sonication (spectrum 1 in **Figure 3**).

Although cavitation bubble dynamics close to solid surfaces has been given particular attention [68], quite little is known about the streaming along the surface. Therefore, in attempting to explain the removal mechanism behind the cleaning effect observed in **Figure 3** there may be several potential ways. One is that the pressure gradients due to bubble implosion and acoustic streaming would bombard and remove organic contaminants on the silicon surface. The other is that some excited oxygen atoms produced by the sonochemical decomposition of the water adhere to the organic compounds, oxidize them finally decomposing into H_2O, O_2, H_2, CO and CO_2, having high vapor pressures allowing the lift-off from the wafer surface [68].

Typical forward and reverse bias $I - V$ characteristics of the wafers with and without organic contaminants are plotted in **Figure 4**. Here, distilled water and piranha (3:1 volume solution of H_2SO_4 and 30%-H_2O_2) are used as a cleaning liquid (curve 2 compared with curves 3 and 4 in **Figure 4**), and both chemical and sonochemical cleaning processes are contrasted (curve 3 compared with curve 4). It is interesting that the cleanings cause an overall decrease in the current through the wafer. This can, in part, be described by the removal of the organic contaminants from the wafer and appropriate quenching of the leaky currents between the basal wafer surfaces. The ultrasonic effect in piranha (curve 4 in **Figure 4**) is obviously greater than that in water (curve 2), as would be expected in reactive chemical agents (cf. curve 2 in **Figure 4**).

Perhaps it is best noted here that the cavitation processing affects a sub layer region beneath the wafer surface. Therefore, the air/oxide and oxide/wafer surface state or interface trap densities could be reduced significantly by this processing step.

This would have a similar effect on the photovoltaic response of the wafers since the photo-induced charge carriers are separated in the electric field of the surface space charge region. These carriers would partially screen the fixed surface or interface state charge thus reducing the surface band bending.

As one of the earliest attempt to manipulate the surface photovoltage, **Figure 5** illustrates the sonication effect on the SPV decays. The decay is seen to be faster for

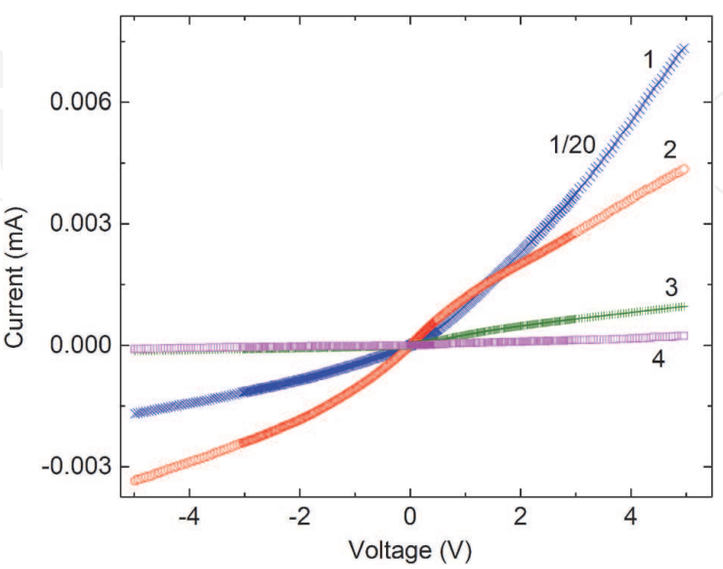

Figure 4.
$I - V$ curves of the Au Schottky contact to n-Si wafer, as-purchased (1), ultrasonically cleaned in distilled water (2), chemically (3) and ultrasonically (4) processed in a piranha bath. In each case, the cleaning time is 60 min. Reprinted with permission from Podolian A, Nadtochiy A, Kuryliuk V, Korotchenkov O, Schmid J, Drapalik M, Schlosser V. Solar Energy Materials and Solar Cells. 2011;95:765–772. Copyright 2010, Elsevier.

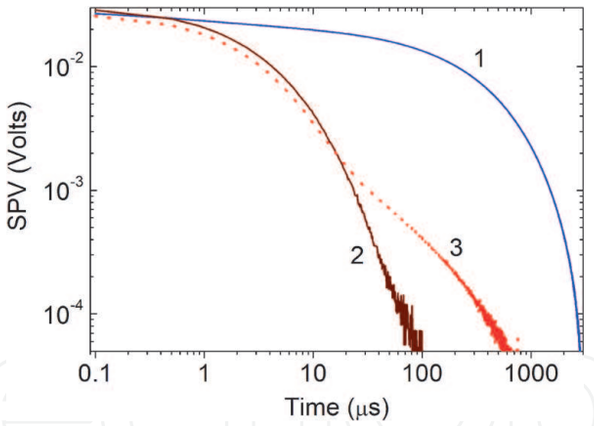

Figure 5.
SPV decays of n-Si, as-purchased (curve 1), ultrasonically cleaned in distilled water for 60 (2) and 120 (3) min. Reprinted with permission from Podolian A, Nadtochiy A, Kuryliuk V, Korotchenkov O, Schmid J, Drapalik M, Schlosser V. Solar Energy Materials and Solar Cells. 2011;95:765–772. Copyright 2010, Elsevier.

ultrasonically cleaned wafer (curve 2 compared with curve 1 in **Figure 5**), which can simply be attributed to an increased density of unsaturated dangling bonds on the wafer surface due to the cavitation-induced local removal of oxide from the silicon surface.

For sonication times increasing up to 90–150 min, the SPV decay is slightly worsened. For example, curve 3 in **Figure 5** exhibits a long-tail decay constituent at time instants greater than ≈20 μs. The involvement of the above surface states and interface traps is therefore reasonable to assume. In this context, for the initial decays at $t < 10$ μs, when the injected carrier concentration is large compared with the density of the trapping centers N_t, the recombination centers mainly determine the excess carrier lifetime. Once the concentration of these carriers becomes exceedingly small, particularly compared with N_t (at $t > 20$ μs, curve 3 in **Figure 5**), the SPV decay is determined by N_t. The initial decays at $t \leq 10$ μs in curves 2 and 3 are nearly identical, giving some indication of the importance of this cavitation processing step in obtaining clean wafer surfaces. Based upon these results, surface and interface trap generation is likely to be significant at prolonged sonication times, greater than 60–90 min.

5. Sonochemical passivation of Si and SiGe

A cogent resource for the burgeoning field of the surface passivation coating utilizing hydrocarbon chains [69], which can reduce the density of surface states and increase the recombination lifetime of the majority carriers. Different organic solvents can be used in practical ways for these purposes such as chloroform ($CHCl_3$) and dichloromethane (CH_2Cl_2). For example, silicone polymers were grown on the Si surfaces with gaseous $CHCl_3$ and Cu catalyst [70], brominated aromatic moieties were successfully prepared from KBr/H_2O_2 in sonochemically treated chloroform [71]. Recent work in applying ultrasound to chemical reactions demonstrates the promise of the sonochemical approach, yet the bromination of aromatic compounds is not achieved with simple mechanical stirring replacing sonication.

This topic is covered in more detail below for two types of samples. Type A sample is a Ge_xSi_{1-x} alloy layer, 100 nm thick, grown on a p-doped Cz-Si wafer. Type B sample is obtained by coating sample A with a 10-nm thick a-Si layer (see **Figure 6**). The Ge content x in the Ge_xSi_{1-x} layers is about 30 at.%.

In order to give an illustrating example for the differences in the effective lifetime τ_{eff}, quasi-steady-state measurements (QSSPC) [72] done in a-Si/Ge_xSi_{1-x}/Si sample are plotted in **Figure 7**. Here, an effective minority carrier lifetime τ_{eff} is obtained from the given by

$$J_{ph} = \frac{\Delta n e W}{\tau_{eff}}, \tag{5}$$

where J_{ph} is the photogenerated current density and Δn is the excess carrier density. At low values of Δn ranging from about 10^{12} to 10^{13} cm^{-3}, **Figure 7(b)** shows≈ 4 times increase in the lifetime due to ultrasonic processing in chloroform (closed circles compared with open circles).

Regarding the role of amorphous Si coating layer (in sample B) and ultrasonic processing on the photovoltaic behavior, one can distinguish several maps of the surface-distributed SPV amplitudes U_0 and decay times τ shown in **Figures 8** and **9**.

It is seen in **Figure 8** that both the U(0) and τ distributions narrow but shift to smaller values once the Ge_xSi_{1-x}/Si structure (sample A) has been coated with a-Si layer (sample B). Faster decays in a-Si/Ge_xSi_{1-x}/Si can be accounted for by an increased number of fast recombination canters in sample B due to the deposited amorphous Si layer, which typically reduces the amplitude of the SPV response.

It is also seen in **Figure 8** that the sonication in chloroform allows for improved SPV performance. Indeed, the SPV decays are spread over much longer time scales to enlarge the SPV amplitude U_0 up to about 50% can be realized in samples, as observed in appropriate distributions, which are marked by B-sono and A-sono in **Figure 8**.

This effect is not pronounced in the samples sonochemically processed in distilled water; see **Figure 9**. Although the distributions of U_0 narrow, the SPV amplitude is itself quenched in the samples treated in distilled water (upper distributions in **Figure 9**). However, similar sonication-affected SPV decay dynamics is observed both in chloroform and distilled water (lower distributions in **Figures 8** and **9**).

The examples in water demonstrate that sonication provides a convenient tool to achieve surface cleaning, as reported previously [7, 73]. In this case, the assumption is based on the fact that (i) the cavitating bubbles are capable of locally removing the surface oxide layer affecting the dangling bonds on the bare Si surface, and (ii) the oxygen and hydrogen, decomposed in water by the presence of local strain fields and elevated temperatures inside a cavitating bubble, can micro-precipitate the Si wafer thus changing the recombination rate. These insights, combined with

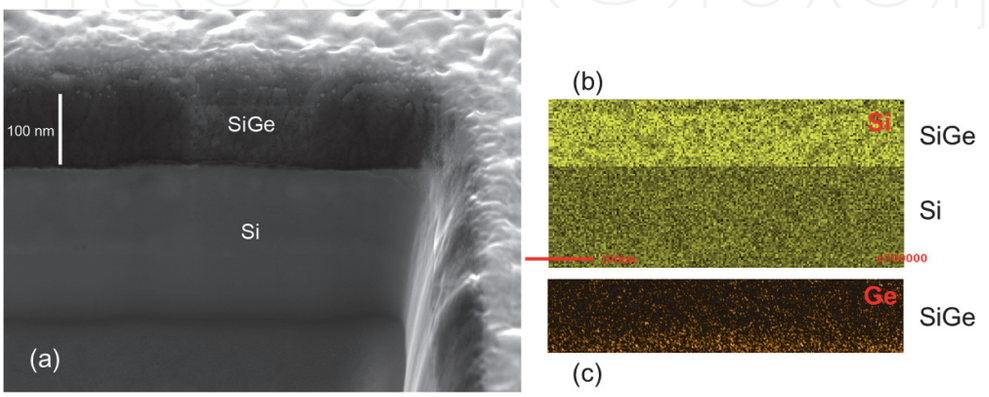

Figure 6.
(a) Cross-sectional scanning electron microscope (SEM) image of a Ge_xSi_{1-x} on Si layer covered with a 10 nm thick a-Si (sample B). (b) and (c) distributions of Si and Ge atoms near the interface mapped using a scanning auger microscopy technique. Reproduced with permission from Nadtochiy A, Korotchenkov O, Schlosser V. Physica Status Solidi (a). 2019;216:1900154. Copyright 2019, Wiley-VCH Verlag GmbH & Co. KGaA.

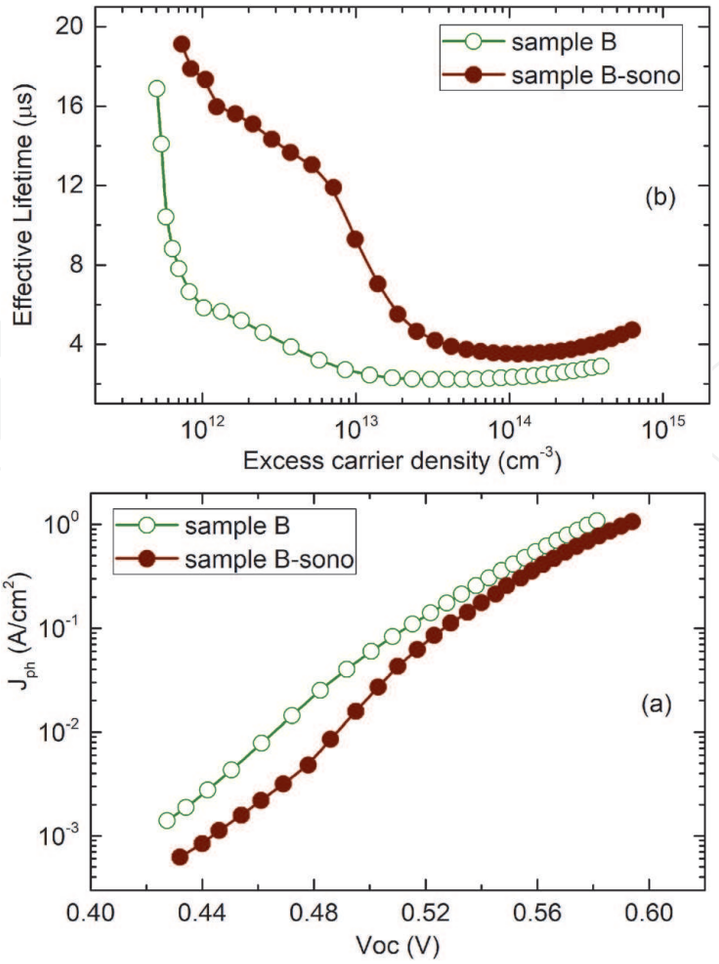

Figure 7.
Current–voltage curve (a) and variation of the effective lifetime τ_{eff} with excess carrier density Δn (b) for sample B before (open circles) and after sonication in chloroform (closed circles). Reproduced with permission from Nadtochiy A, Korotchenkov O, Schlosser V. Physica Status Solidi (a). 2019;216:1900154. Copyright 2019, Wiley-VCH Verlag GmbH & Co. KGaA.

complementary ultrasonic techniques that employ reactant solutions, make a significant contribution to developing a detailed picture of ultrasonic processing.

With respect to the reactant solutions that can be used, recent investigations report that SPV signal in Si can be significantly enhanced, by almost an order of magnitude, due to ultrasonic treatments in dichloromethane. Similar effect in CH_2Cl_2 can be observed for Ge_xSi_{1-x} surfaces exhibiting a 50% increase in the SPV amplitude [74].

The operating frequency range of sonochemical apparatus is typically up to dozens of kHz. A general working principle, which follows from the above guidelines, relies upon a specific assumption that the size of the cavitation bubble is inversely related to the frequency of ultrasound. Therefore, because the bubble size drops with increasing the ultrasonic frequency and the bubble implosions become less violent, the energy released by each imploding cavitation bubble decreases with the ultrasonic frequency. However, the number of the imploding events increases due to increased number of sound waves passing through the liquid at a higher frequency [60].

One may compare the data obtained in Ge_xSi_{1-x} with lower- and higher-frequency sonochemical processing in dichloromethane at about 25 kHz and 400 kHz, respectively. Etching in HF makes initial single-exponential decay nearly double-exponential. Sonication at 25 kHz slightly slows down the tail component of the decay while the higher-frequency processing at 400 kHz turns the SPV decay back into nearly single-exponential form.

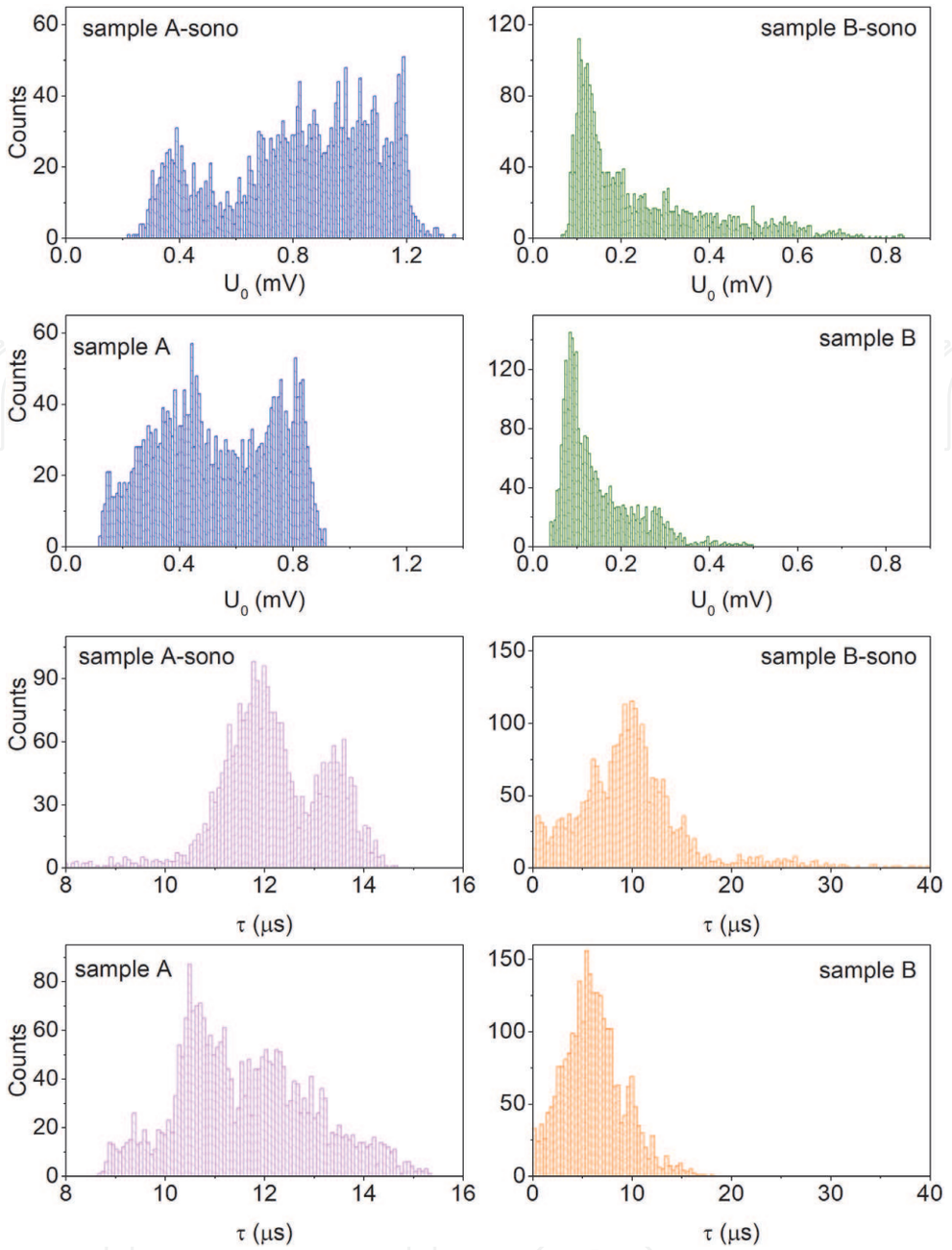

Figure 8.
Probability of occurrences of particular values of the SPV amplitude U_o and decay time τ in samples a (Ge_xSi_{1-x}/Si) and B (a-Si/Ge_xSi_{1-x}/Si), which are measured by surface mappings of the SPV decays. The distributions marked by "sono" are taken after sonochemical treatment in chloroform during 1 min. Reproduced with permission from Nadtochiy A, Korotchenkov O, Schlosser V. Physica Status Solidi (a). 2019;216:1900154. Copyright 2019, Wiley-VCH Verlag GmbH & Co. KGaA.

The likely mechanism that has come to describe the observations is based on that both chloroform and dichloromethane can act as carbon sources. Being decomposed into hydrocarbon species due to extreme conditions in the solvents and at the etchant/solid interfaces, the sonicated reactants seem to saturate the dangling bonds revealed on the surface of Si and Ge_xSi_{1-x} alloys and hence to passivate the surface [14].

This is in accord with previous reports on the thermal decomposition of chloroform, which results in by-products of CCl_2, C_2Cl_4, Cl, H and HCl. When they react with metal (M) atoms, the reactions pathways are [75, 76].

$$CHCl_3(+M) \rightarrow CCl_2 + HCl\ (+M), \tag{6}$$

$$CCl_2 + CCl_2 \rightarrow C_2Cl_2 + Cl + Cl, \tag{7}$$

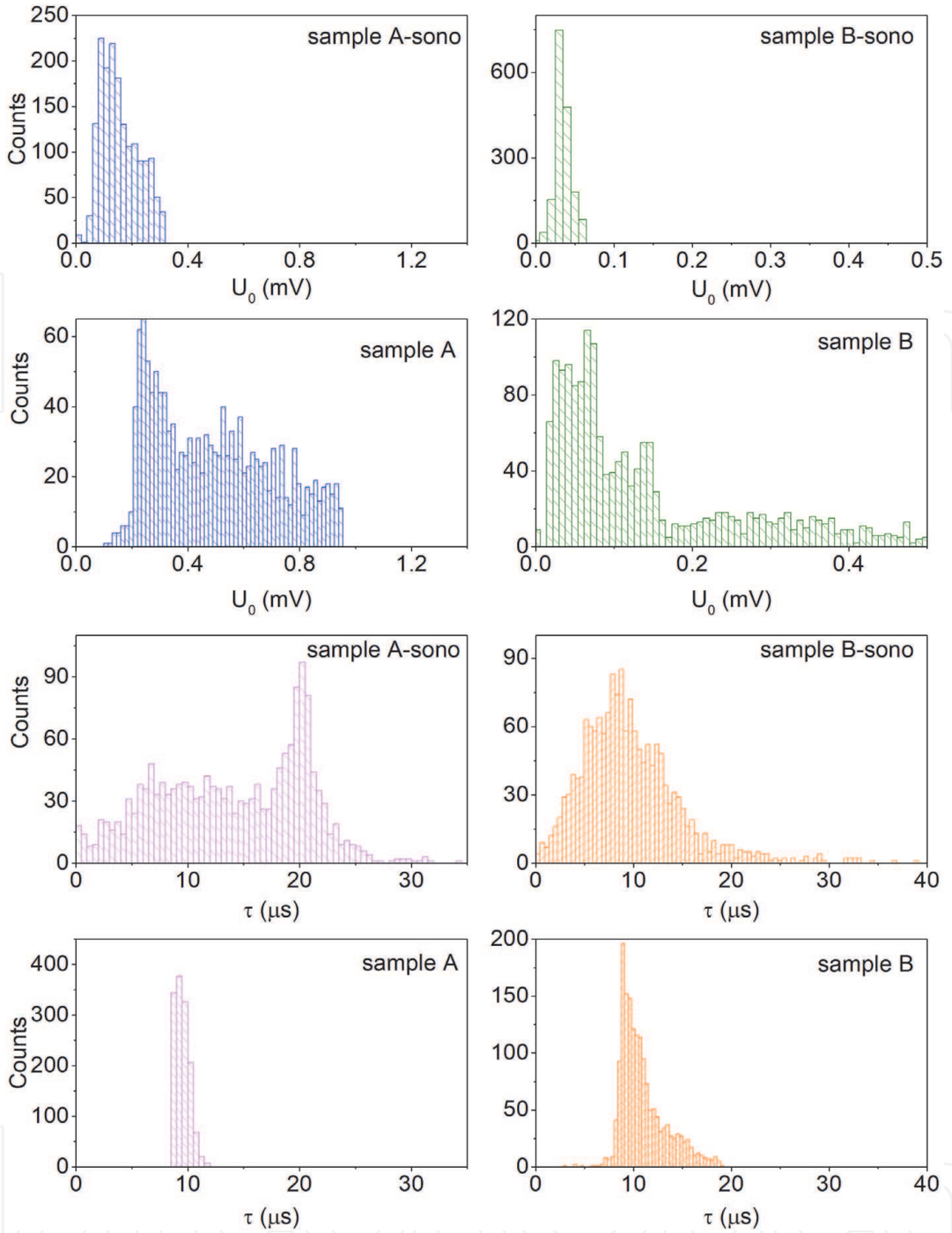

Figure 9.
Probability of occurrences of particular values of the SPV amplitude U_0 and decay time τ in samples a (Ge_xSi_{1-x}/Si) and B (a-Si/Ge_xSi_{1-x}/Si), which are measured by surface mappings of the SPV decays. The distributions marked by "sono" are taken after sonochemical treatment in distilled water during 1 min. Reproduced with permission from Nadtochiy A, Korotchenkov O, Schlosser V. Physica Status Solidi (a). 2019;216:1900154. Copyright 2019, Wiley-VCH Verlag GmbH & Co. KGaA.

$$CCl_2 + M \rightarrow CCl + Cl + M, \tag{8}$$

$$CCl_2 + CCl_2 + M \rightarrow C_2Cl_4 + M, \tag{9}$$

$$HCl + M \rightarrow H + Cl + M, \tag{10}$$

The first reaction step given by Eq. (6) is the decomposition of $CHCl_3$, which is followed by secondary decomposition reactions in Eqs. (7)–(10).

The usual analysis approach for high temperatures achieved during the sonication process involves steps of radical formation, e.g., C_2 radicals:

$$CCl + CCl \rightarrow C_2 + Cl + Cl, \quad (11)$$

$$C_2Cl_2 \rightarrow C_2 + Cl + Cl, \quad (12)$$

Therefore, employing chloroform $CHCl_3$ or dichloromethane CH_2Cl_2, one gets the Si-H and C-Cl bonds that react yielding C-H species. This, in turn, resembles the chlorination/alkylation process that forms Si–alkyl converting Si–H into Si–C_nH_{2n+1} ($n \geq 1$). The alkyl chains on Si surfaces are known to provide low surface recombination velocities [77] thus featuring effective Si surface passivation [78].

In the model presented in **Figure 10**, presumed chemical reactions for the sonochemical surface passivation are made available. The above analysis assumes that the Si–H bond on the surface breaks up at high local temperatures and pressures inside the cavitation bubble. This produces highly reactive Si and Ge dangling bonds, as shown in **Figure 10(a)**. Being short-lived, they quickly react with the sonicated chloroform molecules. Next, molecular hydrocarbon and chlorine atoms cover the a-Si or Ge_xSi_{1-x} surface, as shown in **Figure 10(b)**. The wavy arrow illustrates that Si atoms can be released from the surface due to carbon atoms decomposed from chloroform (or dichloromethane). Finally, these carbon atoms at the surface create Si–C bonds and dangling carbon bonds being then saturated by the atoms of H and Cl. Some of them can meet activated carbon-containing molecules to form Si–C bonds.

In order to obtain the signatures of the chemical constituents, Fourier transformed-infrared (FTIR) spectroscopy is usually applied. FTIR transmittance spectra are shown in **Figure 11**. Among prominent infrared absorption peaks related to the Si–Si, Si–O, Ge–Ge, Ge–O and Ge–O–Si vibration modes, there are resolved bulk-like Si–H and $Si–H_2$ stretching modes at about 2000 and 2090 cm^{-1}, respectively, as well as a weak shoulder near 1880 cm^{-1} related to Ge–H vibrations [79, 80]. These results indicate that Si-H hydrides are present in the deposited a-Si and Ge_xSi_{1-x} films.

One also finds a spectral feature at about 670 cm^{-1} (arrow in the left-hand panel of **Figure 11**). This obviously strengthens in the hydrogenated a-Si film (spectrum 3). To account for this enlargement, one has to assume that this feature is related to the hydrogen complexes. In clear accord, the wagging modes near 640 cm^{-1} can be due to three bonding units of $Si–H_n$ (n = 1, 2, 3) [81]. It is seen in spectrum 4 of **Figure 11** that the sonication quenches the 670 cm^{-1}, which is indicative of the

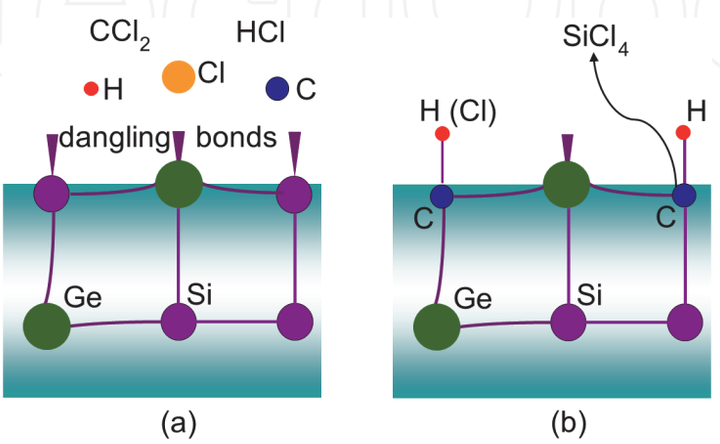

Figure 10.
How to passivate SiGe surface using chloroform reactants H, Cl, C, CCl2, HCl released in Eqs. (6)–(12). These remove Si atoms on the surface and saturate the dangling bonds. Reproduced with permission from Nadtochiy A, Korotchenkov O, Schlosser V. Physica Status Solidi (a). 2019;216:1900154. Copyright 2019, Wiley-VCH Verlag GmbH & Co. KGaA.

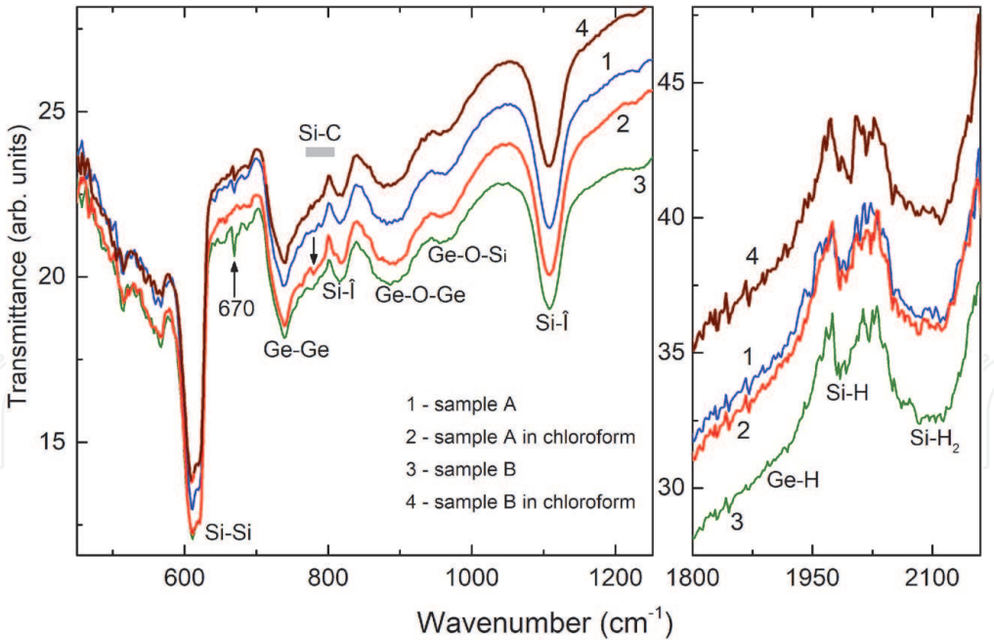

Figure 11.
FTIR spectra of samples Ge_xSi_{1-x}/Si (curve 1) and a-Si/Ge_xSi_{1-x}/Si (3), taken before ultrasonic processing and the ones obtained after the treatment in chloroform – Spectra 2 and 4, respectively. Reproduced with permission from Nadtochiy A, Korotchenkov O, Schlosser V. Physica Status Solidi (a). 2019;216:1900154. Copyright 2019, Wiley-VCH Verlag GmbH & Co. KGaA.

removal of H from the coating layers due to ultrasonic processing, supporting the pictorial view given in **Figure 10**.

6. Conclusions

Two techniques related to ultrasonic cleaning of Si wafers and sonochemical modification of Si, SiGe and a-Si/SiGe surfaces in hydrocarbon solutions of chloroform ($CHCl_3$) and dichloromethane (CH_2Cl_2) are outlined.

In spite of our lack of knowledge of the exact sonication mechanisms even in distilled water, this research field can be considered to be among potential candidates to develop a new class of environmental friendly cleaning steps in silicon-based technologies. Some progress has recently been made in understanding a unique potential capability of sonicated water in Si wafer cleaning processes. The underlying mechanisms related to the fundamental properties of cavitation and bubble implosion events, the role of a thin interphase layer between the bubble and the surface placed in the sonicated liquid can offer new far-reaching implications and importance for heterogeneous liquid–solid systems.

It is demonstrated that organic particle contaminants are effectively removed during the kHz-frequency sonication of crystalline Si wafers in distilled water over the first 40–60 min. When ultrasonically processing the wafers for treatment times less than ≈60 min at the peak acoustic intensity of about 400 W/cm^2, the dangling bonds at the air/oxide and oxide/wafer interface can be activated. That affects barriers of the free carrier migration at the interfaces, as revealed by the current–voltage curves, and acts as recombination centers, accelerating the surface photovoltage decays. A healing of the bonds may occur at longer cleaning times (from 60 to 120 min) with a partial recovery of the interfaces and a consequent reversing of the observed changes. The potential of using distilled water in environmental friendly and non-toxic ultrasonic cleaning step in crystalline Si wafer preparation is addressed.

In fact, the studies described above do not reveal information about the full complexity of subsurface defect distribution effects. Therefore, there remains a wide number of uncertainties, e.g., the fundamental problem of whether or not the ultrasonic processing exploiting high acoustic powers is capable of promoting effective cleaning without surface deterioration effects.

To improve the photovoltaic response of Si wafers, SiGe and amorphous silicon (a-Si)/SiGe surfaces, a sonochemical treatment in hydrocarbon solutions of chloroform ($CHCl_3$) and dichloromethane (CH_2Cl_2) can be employed. The use of the sonochemical reaction slows down the observed surface photovoltage decay and enhances its magnitude in SiGe and a-Si/SiGe thin layers grown on Si. The average surface-integrated photovoltage and decay time can increase up to 50%. This effect is not observed in distilled water, indicative of the fact that CH-containing radicals can lead to the observed improvements. It is suggested that the effect can be explained as follows. The hydrocarbon solution is decomposed and produces hydrocarbon chains, which are then decomposed further away into hydrogen and carbon. The reactive Si dangling bonds revealed on the surface of Si, a-Si or SiGe alloy layers are saturated by the hydrocarbon species to passivate the surface.

More work needs still to be done beyond the description of a very few links that have been highlighted above. In particular, the following experiments could pave the way for new mechanisms of surface passivation, activation of the interphase regions dangling bonds as well as cleaning of surfaces due to the ultrasonic processing.

Acknowledgements

The work at Kyiv was funded by the Ministry of Education and Science of Ukraine (0119U100303). Financial support from the University of Vienna is also acknowledged.

Conflict of interest

The authors declare no conflict of interest.

IntechOpen

IntechOpen

Author details

Andriy Nadtochiy[1], Artem Podolian[1], Oleg Korotchenkov[1] and Viktor Schlosser[2*]

1 Faculty of Physics, Taras Shevchenko National University of Kyiv, Kyiv, Ukraine

2 Department of Electronic Properties of Materials, Faculty of Physics, University of Vienna, Austria

*Address all correspondence to: viktor.schlosser@univie.ac.at

IntechOpen

© 2021 The Author(s). Licensee IntechOpen. This chapter is distributed under the terms of the Creative Commons Attribution License (http://creativecommons.org/licenses/by/3.0), which permits unrestricted use, distribution, and reproduction in any medium, provided the original work is properly cited. CC BY

References

[1] Suslick KS. Sonochemistry. Science. 1990;247:1439–1445. DOI: 10.1126/science.247.4949.1439

[2] Suslick KS, Nyborg WL. Ultrasound: Its chemical, physical and biological effects. The Journal of the Acoustical Society of America. 1990;87:919–920. DOI: 10.1121/1.398864

[3] Gedanken A, Perelshtein I. Power ultrasound for the production of nanomaterials. In: Gallego-Juárez JA, Graff KF, editors. Power ultrasonics. Applications of high-intensity ultrasound. Amsterdam: Woodhead Publishing; 2015. p. 543–576. DOI: 10.1016/B978-1-78242-028-6.00018-1

[4] Sáez V, Mason TJ. Sonoelectrochemical synthesis of nanoparticles. Molecules. 2009;14: 4284–4299. DOI: 10.3390/molecules14104284

[5] Cobley A, Mason T. The evaluation of sonochemical techniques for sustainable surface modification in electronic manufacturing. Circuit World. 2007;33:29–34. DOI: 10.1108/03056120710776997

[6] Paniwnyk L, Cobley A. Ultrasonic surface modification of electronics materials. Physics Procedia. 2009;3: 1103–1108. DOI: 10.1016/j.phpro.2010.01.230

[7] Nadtochiy A, Podolian A, Korotchenkov O, Schmid J, Kancsar E, Schlosser V. Water-based sonochemical cleaning in the manufacturing of high-efficiency photovoltaic silicon wafers. Physica Status Solidi C. 2011;8:2927–2930. DOI: 10.1002/pssc.201084062

[8] Arruda LB, Orlandi MO, Lisboa-Filho PN. Morphological modifications and surface amorphization in ZnO sonochemically treated nanoparticles. Ultrasonics Sonochemistry. 2013;20: 799–804. DOI: 10.1016/j.ultsonch.2012.11.013

[9] Kang B-K, Kim M-S, Park J-G. Effect of dissolved gases in water on acoustic cavitation and bubble growth rate in 0.83 MHz megasonic of interest to wafer cleaning. Ultrasonics Sonochemistry. 2014;21:1496–1503. DOI: 10.1016/j.ultsonch.2014.01.012

[10] Savkina RK, Smirnov AB. Structured silicon surface via cavitation processing for the photovoltaic and biomedical application. In: Fesenko O, Yatsenko L, editors. Nanophysics, Nanophotonics, Surface Studies, and Applications. Springer Proceedings in Physics, v. 183; 2015. p. 291–303. DOI: 10.1007/978-3-319-30737-4_241

[11] Savkina RK, Gudymenko AI, Kladko VP, Korchovyi AA, Nikolenko AS, Smirnov AB, Stara TR, Strelchuk VV. Silicon substrate strained and structured via cavitation effect for photovoltaic and biomedical application. Nanoscale Research Letters. 2016;11:183. DOI: 10.1186/s11671-016-1400-2

[12] Skorb EV, Möhwald H. Ultrasonic approach for surface nanostructuring. Ultrasonics Sonochemistry. 2016;29: 589–603. DOI: 10.1016/j.ultsonch.2015.09.003

[13] Bai F, Wang L, Saalbach K-A, Twiefel J. A novel ultrasonic cavitation peening approach assisted by water jet. Applied Sciences. 2018;8:2218. DOI: 10.3390/app8112218

[14] Nadtochiy A, Korotchenkov O, Schlosser V. Sonochemical modification of SiGe layers for photovoltaic applications. Physica Status Solidi A. 2019;216:1900154. DOI: 10.1002/pssa.201900154

[15] May GS, Spanos CJ. Fundamentals of semiconductor manufacturing and

process control. New Jersey: Wiley; 2006. 463 p. ISBN: 978–0–471-78406-7

[16] De Wolf S, Descoeudres A, Holman ZC, Ballif C. High-efficiency silicon heterojunction solar cells: A review. Green. 2012;2:7–24. DOI: 10.1515/green-2011-0018

[17] Schroder DK. Semiconductor Material and Device Characterization. 3rd ed. Hoboken, New Jersey: Wiley; 2006. 790 p. ISBN: 978–0–471-73906-7

[18] Deal BE, Grove AS. General relationship for the thermal oxidation of silicon. Journal of Applied Physics. 1965; 36:3770–3778. DOI: 10.1063/1.1713945

[19] Aberle AG, Hezel R. Progress in low-temperature surface passivation of silicon solar cells using remote-plasma silicon nitride. Progress in Photovoltaics. 1997;5:29–50. DOI: 10.1002/(SICI)1099-159X(199701/02)5:1<29::AID-PIP149>3.0.CO;2-M

[20] Benick J, Zimmermann K, Spiegelmann J, Hermle M, Glunz SW. Fundamental losses in solar cells. Progress in Photovoltaics. 2011;19:361–365. DOI: 10.1002/pip.1024

[21] Pankove JI, Tarng ML. Amorphous silicon as a passivant for crystalline silicon. Applied Physics Letters. 1979;34: 156–157. DOI: 10.1063/1.90711

[22] Lin Y, Feng M, Wang Z, Zeng Y, Liao M, Gong L, Yan B, Yuan Z, Ye J. Excellent passivation with implied open-circuit voltage of 710 mV for p-type multi-crystalline black silicon using PECVD grown a-Si:H passivation layer. Solar Energy. 2020; 211:753–758. DOI: 10.1016/j.solener.2020.10.023

[23] Balaji P, Dauksher WJ, Bowden SG, Augusto A. Improving surface passivation on very thin substrates for high efficiency silicon heterojunction solar cells. Solar Energy Materials and Solar Cells. 2020;216:110715. DOI: 10.1016/j.solmat.2020.110715

[24] Schmidt J, Peibst R, Brendel R. Surface passivation of crystalline silicon solar cells: Present and future. Solar Energy Materials and Solar Cells. 2018;187: 39–54. DOI: 10.1016/j.solmat.2018.06.047

[25] Angermann H. Characterization of wet-chemically treated silicon interfaces by surface photovoltage measurements. Analytical and Bioanalytical Chemistry. 2002;374:676–680. DOI: 10.1007/s00216-002-1450-4

[26] Angermann H, Henrion W, Röseler A. Wet-chemical conditioning of silicon: Electronic properties correlated with the surface morphology. In: Nalwa HS, editor. Silicon-Based Materials and Devices. San Diego: Academic Press; 2001; Volume 1, p. 268–299. DOI: 10.1016/B978-012513909-0/50009-X

[27] Podolian A, Nadtochiy A, Korotchenkov O, Romanyuk B, Melnik V, Popov V. Enhanced photoresponse of Ge/Si nanostructures by combining amorphous silicon deposition and annealing. Journal of Applied Physics. 2018;124:095703. DOI: 10.1063/1.5029948

[28] Coignus J, Baudrit M, Singer J, Lachaume R, Muñoz D, Thony P. Key issues for accurate simulation of a-Si:H / c-Si heterojunction solar cells. Energy Procedia. 2011;8:174–179. DOI: 10.1016/j.egypro.2011.06.120

[29] Duttagupta S, Lin F, Wilson M, Boreland MB, Hoex B, Aberle AG. Extremely low surface recombination velocities on low-resistivity n-type and p-type crystalline silicon using dynamically deposited remote plasma silicon nitride films. Progress in Photovoltaics. 2014;22: 641–647. DOI: 10.1002/pip.2320

[30] Koch C, Ito M, Schubert M. Solar Energy Materials and Solar Cells. 2001;

68:227–236. DOI: 10.1016/S0927-0248(00)00249-X

[31] Fujiwara H, Kondo M. Impact of epitaxial growth at the heterointerface of a-Si:H/c-Si solar cells. Applied Physics Letters. 2007; 90:013503. DOI: 10.1063/1.2426900

[32] De Wolf S, Kondo M. Abruptness of a-Si:H/c-Si interface revealed by carrier lifetime measurements. Applied Physics Letters. 2007;90:042111. DOI: 10.1063/1.2432297

[33] Fujiwara H, Kaneko T, Kondo M. Application of hydrogenated amorphous silicon oxide layers to c-Si heterojunction solar cells. Applied Physics Letters. 2007;91:133508. DOI: 10.1063/1.2790815

[34] Mueller T, Schwertheim S, Scherff M, Fahrner WR. High quality passivation for heterojunction solar cells by hydrogenated amorphous silicon suboxide films. Applied Physics Letters. 2008;92:033504. DOI: 10.1063/1.2837192

[35] Mueller T, Schwertheim S, Fahrner WR. Crystalline silicon surface passivation by high-frequency plasma-enhanced chemical-vapor-deposited nanocomposite silicon suboxides for solar cell applications. Journal of Applied Physics. 2010;107:014504. DOI: 10.1063/1.3264626

[36] Rattanapan S, Watahiki T, Miyajima S, Konagai M. Improvement of rear surface passivation quality in p-type silicon heterojunction solar cells using boron-doped microcrystalline silicon oxide. Japanese Journal of Applied Physics. 2011;50:082301. DOI: 10.1143/JJAP.50.082301

[37] Xiao SQ, Xu S, Zhou HP, Wei DY, Huang SY, Xu LX, Sern CC, Guo YN, Khan S. Amorphous/crystalline silicon heterojunction solar cells via remote inductively coupled plasma processing. Applied Physics Letters. 2012;100:233902. DOI: 10.1063/1.4721642

[38] Suslick KS, Didenko Y, Fang MM, Hyeon T, Kolbeck KJ, McNamara III WB, Mdleleni MM, Wong M. Acoustic cavitation and its chemical consequences. Philosophical Transactions of the Royal Society A: Mathematical, Physical and Engineering Sciences. 1999;357:335–353. DOI: 10.1098/rsta.1999.0330

[39] Leighton TG. The Acoustic Bubble. London: Academic; 1994. 613 p. ISBN: 0–12–441920-8

[40] Yasui K. Influence of ultrasonic frequency on multibubble sonoluminescence. The Journal of the Acoustical Society of America. 2002;112:1405–1413. DOI: 10.1121/1.1502898

[41] Gutierrez M, Henglein A, Ibanez F. Radical scavenging in the sonolysis of aqueous solutions of iodide, bromide, and azide. The Journal of Physical Chemistry. 1991;95:6044–6047. DOI: 10.1021/j100168a061

[42] Kumar RV, Koltypin Yu, Xu XN, Yeshurun Y, Gedanken A, Felner I. Fabrication of magnetite nanorods by ultrasound irradiation. Journal of Applied Physics. 2001;89:6324–6328. DOI: 10.1063/1.1369408

[43] Prasanthkumar KP, Rayaroth MP, Alvarez-Idaboy JR. Insights into the mechanism of hydroxyl radical mediated oxidations of 2-aminopurine: A computational and sonochemical product analysis study. The Journal of Physical Chemistry B. 2020;124:6245–6256. DOI: 10.1021/acs.jpcb.0c03974

[44] González-García J, Sáez V, Tudela I, Díez-Garcia MI, Esclapez MD, Louisnard O. Sonochemical treatment of water polluted by chlorinated organocompounds. A review. Water. 2010;2:28–74. DOI: 10.3390/w2010028

[45] Xu H, Zeiger BW, Suslick KS. Sonochemical synthesis of nanomaterials. Chemical Society Reviews. 2013;42:2555–2567. DOI: 10.1039/c2cs35282f

[46] Birkin PR, Power JF, Leighton TG, Vinçotte AML. Cathodic electrochemical detection of sonochemical radical products. Analytical Chemistry. 2002;74:2584–2590. DOI: 10.1021/ac010964o

[47] Suslick KS. Sonochemistry. In: Kirk-Othmer Encyclopedia of Chemical Technology, v. 26. New York: Wiley; 1998. p. 517–541.

[48] Compton RG, Eklund JC, Marken F. Sonoelectrochemical processes. A review. Electroanalysis. 1997;9:509–522. DOI: 10.1002/elan.1140090702

[49] Brett C. Sonoelectrochemistry. In: Vives AA, editor. Piezoelectric Transducers and Applications. Heidelberg, Berlin: Springer-Verlag; 2008; Chapter 15, p. 399–411. DOI: 10.1007/978-3-540-77508-9

[50] Mason TJ, Lorimer JP, Bates DM. Quantifying sonochemistry: casting some light on a 'black art'. Ultrasonics. 1992;30:40–42. DOI: 10.1016/0041-624X(92)90030-P

[51] Kern W. Overview and evolution of silicon wafer cleaning technology. In: Reinhardt KA, Kern W, editors. Handbook of Silicon Wafer Cleaning Technology. 3rd ed. Elsevier: Oxford; 2018. p. 3–85. DOI: 10.1016/B978-0-323-51084-4.00001-0

[52] Chung HY, Kim YH, Cho HY, Lee BY, Yoo HD, Lee SH. Collection efficiency of metallic contaminants on Si wafer by vapor-phase decomposition-droplet collection. Analytical Sciences. 2001;17:653–658. DOI: 10.2116/analsci.17.653

[53] Lee D-H, Kim H-T, Jang S-H, Yi J-H, Choi E-S, Park J-G. Effect of organic acids in dilute HF solutions on removal of metal contaminants on silicon wafer. Microelectronic Engineering. 2018;198:98–102. DOI: 10.1016/j.mee.2018.06.012

[54] Ramappa DA, Henley WB. Effects of copper contamination in silicon on thin oxide breakdown. Journal of the Electrochemical Society. 1999;146:2258–2260. DOI: 10.1149/1.1391924

[55] Lim SW, Machuca F, Liao H, Chiarello RP, Helms RC. Effect of initial Al contamination on ultrathin gate oxides. Journal of the Electrochemical Society. 2000;147:1136–1140. DOI: 10.1149/1.1393325

[56] Ryuta J, Yoshimi T, Kondo H, Okuda H, Shimanuki Y. Adsorption and desorption of metallic impurities on Si wafer surface in SC1 solution. Japanese Journal of Applied Physics. 1992;31:2338–2342. DOI: 10.1143/JJAP.31.2338

[57] Osaka T, Hattori T. Influence of initial wafer cleanliness on metal removal efficiency in immersion SC-1 cleaning: Limitation of immersion-type wet cleaning. IEEE Transactions on Semiconductor Manufacturing. 1998;11:20–24. DOI: 10.1109/66.661280

[58] Kern W, Puotinen DA. Clean solutions based on hydrogen peroxide for use in silicon semiconductor technology. RCA Review. 1970;31:187–206.

[59] Hoefflinger B. ITRS: The international technology roadmap for semiconductors. In: Hoefflinger B, editor. Chips 2020. The Frontiers Collection. Springer: Berlin; 2011. p. 161–174. DOI: 10.1007/978-3-642-23096-7_7

[60] Fuchs FJ. Ultrasonic cleaning and washing of surfaces. In: Gallego-Juárez JA, Graff KF, editors. Power ultrasonics. Applications of high-intensity ultrasound. Amsterdam: Woodhead Publishing; 2015. p. 577–609.

DOI: 10.1016/B978-1-78242-028-6.00019-3

[61] Ellenberger J, van Baten JM, Krishna R. Exploiting the Bjerknes force in bubble column reactors. Chemical Engineering Science. 2005;60: 5962–5970. DOI: 10.1016/j.ces.2005.03.036

[62] Sapozhnikov OA. High-intensity ultrasonic waves in fluids: nonlinear propagation and effects. In: Gallego-Juárez JA, Graff KF, editors. Power ultrasonics. Applications of high-intensity ultrasound. Amsterdam: Woodhead Publishing; 2015. p. 9–35. DOI: 10.1016/B978-1-78242-028-6.00002-8

[63] Gale GW, Busnaina AA. Removal of particulate contaminants using ultrasonics and megasonics: A review. Particulate Science and Technology. 1995;13:197–211. DOI: 10.1080/02726359508906678

[64] Busnaina AA, Gale GW. Roles of cavitation and acoustic streaming in megasonic cleaning, J. Particulate Science and Technology. 1999;17:229–238. DOI: 10.1080/02726359908906815

[65] Kim JM, Kim YK. The enhancement of homogeneity in the textured structure of silicon crystal by using ultrasonic wave in the caustic etching process. Solar Energy Materials and Solar Cells. 2004;81:239–247. DOI: 10.1016/j.solmat.2003.11.019

[66] Ohl C-D, Arora M, Dijkink R, Janve V, Lohse D. Surface cleaning from laser-induced cavitation bubbles. Applied Physics Letters. 2006;89: 074102. DOI: 10.1063/1.2337506

[67] Endo M, Yoshida H, Maeda Y, Miyamoto N, Niwano M. Infrared monitoring system for the detection of organic contamination on a 300 mm Si wafer. Applied Physics Letters. 1999;75: 519–521. DOI: 10.1063/1.124434

[68] Podolian A, Nadtochiy A, Kuryliuk V, Korotchenkov O, Schmid J, Drapalik M, Schlosser V. The potential of sonicated water in the cleaning processes of silicon wafers. Solar Energy Materials and Solar Cells. 2011;95:765–772. DOI: 10.1016/j.solmat.2010.10.019

[69] Heinz H, Pramanik C, Heinz O, Y Ding, Mishra RK, Marchon D, Flatt RJ, Estrela-Lopis I, Llop J, Moya S, Ziolo RF. Nanoparticle decoration with surfactants: Molecular interactions, assembly, and applications. Surface Science Reports. 2017;72:1–58. DOI: 10.1016/j.surfrep.2017.02.001

[70] Swalen JD, Allara DL, Andrade JD, Chandross EA, Garoff S, Israelachvili J, McCarthy TJ, Murray R, Pease RF, JF Rabolt, Wynne KJ, Yu H. Molecular monolayers and films. Langmuir. 1987;3: 932–950. DOI: 10.1021/la00078a011

[71] Lévêque J-M, Fujita M, Bosson A, Sohmiya H, Pétrier C, Komatsu N, Kimura T. Secondary sonochemical effect on Mo-catalyzed bromination of aromatic compounds. Ultrasonics Sonochemistry. 2011;18:753–756. DOI: 10.1016/j.ultsonch.2010.11.006

[72] Sinton RA, Cuevas A. Contactless determination of current–voltage characteristics and minority-carrier lifetimes in semiconductors from quasi-steady-state photoconductance data. Applied Physics Letters. 1996;69:2510–2512. DOI: 10.1063/1.117723

[73] A Nadtochiy, Korotchenkov O, Drapalik M, Schlosser V. Effects of ultrasonic cleaning on carrier lifetimes and photovoltage in monocrystalline silicon. Solid State Phenomena. 2011; 178–179:221–225. DOI: 10.4028/www.scientific.net/SSP.178-179.221

[74] Shmid V, Podolian A, Nadtochiy A, Yazykov D, Semen'ko M, Korotchenkov O. Photovoltaic characterization of Si and SiGe surfaces sonochemically treated in

dichloromethane. Journal of Nano- and Electronic Physics. 2020;12:01023. DOI: 10.21272/jnep.12(1).01023

[75] Kumaran SS, Su M-C, Lim KP, Michael JV, Klippenstein SJ, DiFelice J, Mudipalli PS, Kiefer JH, Dixon DA, Peterson KA. Experiments and theory on the thermal decomposition of $CHCl_3$ and the reactions of CCl_2. Journal of Physical Chemistry A. 1997;101:8653–8661. DOI: 10.1021/jp971723g

[76] Chun YS, Lee ES, Jeong MG, Lim DS. Synthesis and characteristics of chloroform-treated silicon carbide-derived carbon layers. RSC Advances. 2016;6:96669–96675. DOI: 10.1039/C6RA22768F

[77] Royea WJ, Juang A, Lewis NS. Preparation of air-stable, low recombination velocity Si(111) surfaces through alkyl termination. Applied Physics Letters. 2000;77:1988–1990. DOI: 10.1063/1.1312203

[78] Hunger R, Fritsche R, Jaeckel B, Jaegermann W, Webb LJ, Lewis NS. Chemical and electronic characterization of methyl-terminated Si(111) surfaces by high-resolution synchrotron photoelectron spectroscopy. Physical Review B. 2005; 72:045317. DOI: 10.1103/PhysRevB.72.045317

[79] Mui K, Smith FW. Optical dielectric function of hydrogenated amorphous silicon: Tetrahedron model and experimental results. Physical Review B. 1988;38:10623–10632. DOI: 10.1103/PhysRevB.38.10623

[80] Kessels WMM, Marra DC, van de Sanden MCM, Aydil ES. In situ probing of surface hydrides on hydrogenated amorphous silicon using attenuated total reflection infrared spectroscopy. Journal of Vacuum Science & Technology A. 2002;20:781–789. DOI: 10.1116/1.1469012

[81] Brodsky MH, Cardona M, Cuomo JJ. Infrared and Raman spectra of the silicon-hydrogen bonds in amorphous silicon prepared by glow discharge and sputtering. Physical Review B. 1977;16: 3556–3571. DOI: 10.1103/PhysRevB.16.3556